Bioorganic Chemistry 85 (2019) 420–430

Contents lists available at ScienceDirect

Bioorganic Chemistry

journal homepage: www.elsevier.com/locate/bioorg

Synthesis of 1-(α-aminoalkyl)-2-naphthol and α-aminonitrile derivatives with molybdenum Schiff base complex covalently bonded on silica-coated magnetic nanoparticles and DNA interaction study of one type of derivatives using computational and spectroscopic methods

Jamshid Rakhtshah[a], Behrouz Shaabani[a,*], Sadegh Salehzadeh[b], Neda Hosseinpour Moghadam[b]

[a] Department of Inorganic Chemistry, Faculty of Chemistry, University of Tabriz, Tabriz, Iran
[b] Faculty of Chemistry, Bu-Ali Sina University, Hamedan 6517838683, Iran

ARTICLE INFO

Keywords:
Immobilized complexes
1-(α-aminoalkyl)-2-naphthol
Ultrasonication
Molecular docking
DNA interaction

ABSTRACT

An air- and moisture-stable molybdenum Schiff base complexes immobilized on magnetic iron oxide nanoparticles with a core-shell structure was developed for utilization as a new heterogeneous catalyst. The surface, structural and magnetic characteristics of the nanomaterials were characterized by using Fourier transform infrared (FT-IR) spectroscopy, X-ray powder diffraction (XRD), vibrating sample magnetometry (VSM), scanning electron microscopy (SEM), energy dispersive X-ray (EDX) and inductively coupled plasma atomic emission spectroscopy (ICP-AES). In application point of view, an ultrasonic assisted one-pot multicomponent protocol for the synthesis of 1-(α-aminoalkyl)-2-naphthol derivatives have been demonstrated under mild condition with short reaction times, high yields and TON values up to 570. To survey the generality of the procedure, we studied the synthesis of α-aminonitrile derivatives with different aldehydes, trimethylsilyl cyanide (TMSCN) and aniline under the same conditions. Additionally, binding interaction of 1-(phenyl(pyridin-2-ylamino)methyl)naphthalen-2-ol (AMAN-1) with various types of rigid DNA and HSA has been investigated by molecular modeling study. In vitro studies under physiological conditions showed that the desired derivative interacts with calf-thymus DNA (ct-DNA) via an intercalative binding mode.

1. Introduction

From an environmental friendly and cost-effective point of view, facile recovery and recycling of the catalyst are the two most important features in catalytic processes [1]. Due to easier recovery, a lot of research work is focused on the synthesis of new heterogeneous catalysts [2–4]. However, these catalysts are not completely recoverable via filtration or centrifugation after catalytic reactions which lead to loss of solid catalysts in the separation process [5,6]. Hence there is a need to design clean catalysts with high reusability and stability which can overcome these drawbacks. To overcome such limitations, magnetite nanoparticles, especially Fe_3O_4 nanoparticles, have attracted significant interest as the support materials due to their unique physical properties including large surface-to-volume ratio, magnetism and low toxicity. Iron magnetic nanoparticles can be easily synthesized and functionalized and they can be recycled from the reaction medium by an external magnetic field [7,8].

Homogenous transition metal Schiff base complexes have been extensively studied in the field of catalysis reactions [9,10]. The Schiff base complexes used in these reactions are generally ease of preparation and they are nontoxic, air, thermally and moisture stable [11,12]. It should be noted that the mentioned catalysts exhibit high catalytic activity in a wide range of reactions such as epoxidation of olefins, asymmetric ring opening of terminal epoxides, hydrogenation of organic substrates, oxidation reactions and coupling reactions [13–15]. However, these systems have several drawbacks related to the difficulty of catalyst recycling. In order to overcome the aforesaid concerns, various organic/inorganic solid materials have been frequently applied as insoluble support for these complexes [16–20]. In comparison with the other supports, the silica-coated iron oxide particles offer pronounced advantages, like facilitating the grafting of various coupling agents such as linkers, ligands, metals or complexes on their surface through the silanol groups, better dispersion of the catalyst in solvents, great resistance to organic solvents, thermal resistance and better performance in different chemical trans-formations [21].

The Mannich reaction is one of the most important multicomponent

* Corresponding author.
E-mail address: shaabani.b@gmail.com (B. Shaabani).

https://doi.org/10.1016/j.bioorg.2019.01.022
Received 13 September 2018; Received in revised form 3 January 2019; Accepted 9 January 2019
Available online 11 January 2019
0045-2068/

reactions in organic chemistry for the one-pot synthesis of 1-(α-aminoalkyl)-2-naphthols, the so-called Betti bases [22]. Preparation of substituted Betti base derivatives with 1,3-aminooxygenated functional groups are important and attractive due to their interesting catalytic [23], pharmaceutical and biological properties [24]. They are the key precursors for the synthesis of a variety of biologically significant natural products including antibiotics and HIV protease inhibitors [25]. In addition, this type of compounds has showed a high level of catalytic activity as chiral catalysts in the enantioselective alkylation or arylation of benzaldehyde [26]. The three-component typical Betti reaction is a condensation reaction between an aldehyde, ammonia or urea and β-naphthol [27,28]. Recently, a modified method via a three-component condensation of aromatic aldehydes, 2 or 4-aminopyridine and β-naphthol in the presence of MNP-$PhSO_3H$ [29] and {[1,4-DHPyrazine][$C(NO_2)_3]_2$} [30] as catalyst has been reported. Also, there are a couple of papers, which possessed our consideration on the feasibility to dominate the use of catalysts. In the first one, the reaction was performed in the absence of solvents by heating the mixture at 125 °C to generate the corresponding products with good yields [31]. The second one remarked the effect of H_2O as solvent on the reaction at room temperature [32].

To the best of our knowledge, no report has been made so far about the synthesis of 1-(α-aminoalkyl)-2-naphthols catalyzed by supported Schiff base complexes by ultrasonic irradiation. With this view in mind and our studies using a variety of immobilized Schiff base complexes [33–35], we have developed a mild, efficient and environmentally friendly procedure for the one-pot Mannich synthesis of 1-(α-aminoalkyl)-2-naphthols derivatives from the coupling of β-naphthol (1), various aromatic aldehydes (2) and 2, 3 or 4-aminopyridine (3) using molybdenum Schiff base complex immobilized on silica coated Fe_3O_4 as a reusable catalyst (Scheme 1). This novel synthetic method is especially favored because it provides a synergy between immobilized complex on magnetic support and ultrasound irradiation which offers the more advantages compared to the conventional methods reported in the literature. In addition, binding interaction of one selected derivative with various types of rigid DNA and HSA has been investigated by molecular modeling study and also we study DNA interaction of this derivative with calf-thymus DNA (ct-DNA) using spectroscopic methods.

2. Experimental

2.1. General Information

All the commercially available reagents and solvents in the present study were used without further purification. IR spectra were recorded with a Jusco 300 FT-IR instrument in the range 400–4000 cm^{-1}, using KBr pellets. Powder X-ray diffraction patterns were collected with a Bruker D8ADVANCE diffractometer with Cu Kα radiation (λ = 1.5406 Å) at a rate of 0.05°/min from 10° to 90° of 2θ. Field

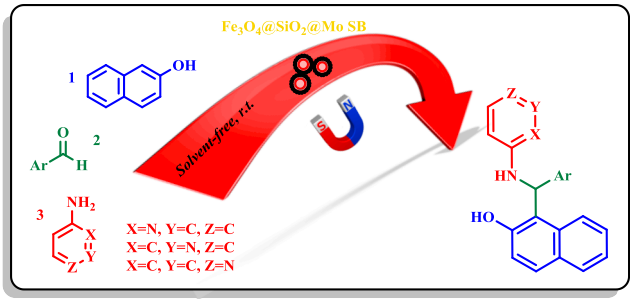

Scheme 1. The synthesis of 1-(α-aminoalkyl)-2-naphthols derivatives using molybdenum complex supported on functionalized Fe_3O_4 magnetite nanoparticles.

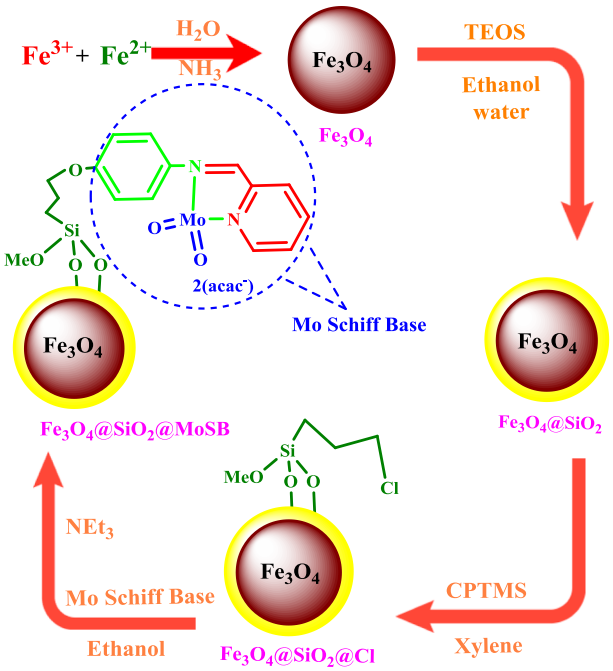

Scheme 2. The sequence of events in the preparation of Fe_3O_4@SiO_2@MoSB.

emission scanning electron microscope (FESEM) was carried out on Philips XL30. Magnetic measurement of materials was investigated with a vibrating sample magnetometer (VSM) (4 in., Daghigh Meghnatis Kashan Co., Kashan, Iran) at room temperature. The ICP analyses were carried out by Perkin-Elmer optima 7300 DV spectrometer. Reaction progress and purity of derivatives were checked by TLC using silica gel SIL G/UV 254 plates. The ^1H NMR (400.13) and ^{13}C NMR (100.62 MHz) spectra were obtained in DMSO-d_6 using a Bruker Avance spectrometer.

A schematic representation for the synthesis of molybdenum Schiff base complex immobilized on silica-coated Fe_3O_4 nanoparticles is shown in Scheme 2.

2.2. Synthesis of iron oxide nanoparticles (Fe_3O_4)

Fe_3O_4 nanoparticles were synthesized by chemical precipitation technique [36]. Aqueous solution of $FeCl_3{\cdot}6H_2O$ and $FeCl_2{\cdot}6H_2O$ salts were mixed in deionized water in 2:1 ratio at 80 °C with rapid addition of NH_4OH under ultrasonication condition to yield a black powder. The precipitate was washed three times with ethanol and deionized water and dried at 60 °C.

2.3. Synthesis of silica coated iron oxide nanoparticles (Fe_3O_4@SiO_2)

For synthesis of silica-coated Fe_3O_4 nanoparticles [37], 2 g of Fe_3O_4 NPs were added to a solution of 100 mL ethanol. The mixture sonicated for 10 min, and then 10 mL of deionized water, 2.5 mL of 25 wt% concentrated aqueous ammonia solution and tetraethylorthosilicate (TEOS) were added in turn. The mixture was stirred for 4 h at room temperature. The brown silica-coated nanoparticles were collected from the solution using a magnet and thoroughly washed with ethanol and deionized water, followed by drying under vacuum overnight.

2.4. Coating iron oxide nanoparticles with chlorosilane coupling agent (Fe_3O_4@SiO_2@Cl)

1 g of silica coated nanoparticles was suspended in a 100 mL xylene solution of 3-chloropropyltrimethoxysilane (CPTMS) (2 mL) under dry nitrogen atmosphere. The mixture was refluxed for 3 h. The precipitate was collected and the nanoparticles were washed with two portions of

xylene (20 mL), and one portion of ethanol (20 mL), before drying under vacuum.

2.5. Synthesis of molybdenum Schiff base complex (MoSB)

The homogeneous Schiff base ligand was synthesized as follows. 2-Formylpyridine (1 mmol) was dissolved in ethanol. Then, a mixture of 4-aminophenol (1 mmol) in ethanol was added, and the mixture was refluxed for 3 h. The mixture was cooled and the resultant solid was separated and washed with ethanol and dried under vacuum. yield: 90%. Then a solution of $MoO_2(acac)_2$ (1 mmol) in absolute ethanol (10 mL) was added to a mixture of the prepared Schiff base ligand (1 mmol) in absolute ethanol (10 mL). The mixture was stirred at 60 °C for 3 h, then filtered, and the precipitate was washed well with absolute ethanol (3 × 10 mL).

2.6. Synthesis of immobilized Mo complexes on silica-coated Fe_3O_4 nanoparticles (Fe_3O_4@SiO_2@MoSB)

The nanoparticles coated with chlrosilane coupling agent were first dispersed with ultrasonication in ethanol, for 10 min and then MoSB (0.5 g) was added to reaction medium and the contents of the flask were refluxed for 12 h. The solid was collected with external magnet, dried at 60 °C, and washed three times with ethanol.

2.7. General procedure for the synthesis of 1-(α-aminoalkyl)-2-naphthol derivatives

A mixture of aromatic aldehydes (1 mmol), β-naphthol (1 mmol; 0.144 g), 2-, 3- or 4-aminopyridine (1 mmol; 0.094 g), and catalyst (6 mg) was exposed to ultrasound irradiation at room temperature for an appropriate time (Table 5). The reaction was monitored by TLC (*n*-hexane/ethyl acetate: 5/2), and ethyl acetate (10 mL) was added to mixture and stirred for 10 min. The catalyst was collected with magnet and washed with ethanol three times, dried in vacuum and reused. The solvent was evaporated under reduced pressure and the crude product was purified by recrystallization from hot ethanol. The products were characterized by IR, ^{1}H and ^{13}C NMR.

***1-((2,4-Dichlorophenyl)(pyridin-2-ylamino)methyl)naphthalen-2-ol* (Table 5, *entry 5*)**: FT-IR (KBr): υ 3388, 3064, 1613, 1511, 1344, 1234 cm^{-1}; ^{1}H NMR (400 MHz, DMSO-d_6) δ_{ppm} 13.93 (s, 1H, −OH), 8.23 (s, 1H, −NH), 8.05 (d, J = 8.5 Hz, 1H, ArH), 7.99 (d, J = 9.2 Hz, 1H, ArH), 7.95 (d, J = 5.4 Hz, 1H, ArH), 7.91 (d, J = 8.8 Hz, 1H, ArH), 7.57 (d, J = 5.8 Hz, 1H, ArH), 7.55 (d, J = 8.5 Hz, 1H, ArH), 7.48 (d, J = 8.8 Hz, 1H, ArH), 7.39 (t, J = 8.0 Hz, 1H, ArH), 7.24 (d, J = 5.8 Hz, 1H, ArH), 7.14 (t, J = 7.4 Hz, 1H, ArH), 7.02 (t, J = 8.6 Hz, 1H, ArH), 6.85 (t, J = 8.5 Hz, 1H, ArH), 6.19 (s, 1H, −CH aliphatic); ^{13}C NMR (101 MHz, DMSO-d_6) δ_{ppm} 143.9, 142.8, 135.6, 132.4, 131.0, 130.6, 130.4, 130.1, 130.0, 128.7, 127.4, 124.8, 124.3, 123.3, 122.6, 118.5, 117.5, 116.4, 114.7, 113.4, 112.0, 35.3.

2.8. Molecular docking

The three-dimensional (3D) structure of 1-(phenyl(pyridin-2-ylamino)methyl)naphthalen-2-ol (AMAN-1) was built, and its geometry was optimized through Hyper Chem version 8 program [38]. The optimized structure of desired derivative was used for the molecular docking simulation (Fig. 1). The crystal structures of the pdb DNAs and HSA used in molecular docking were extracted from Protein Data Bank (http://www.rcsb.org/pdb/home/home.do) and listed in Table 1.

The binding interactions of AMAN-1 with all of the pdb DNA structures and HSA were simulated by molecular docking method using AutoDock 4.0 program [39]. All of the water molecules were removed from the pdb structures and then the polar hydrogen atoms were added. The grid maps of dimensions 60 × 60 × 60 Å and 126 × 126 × 126 Å with a grid-point spacing of 0.375 Å were created respectively for five

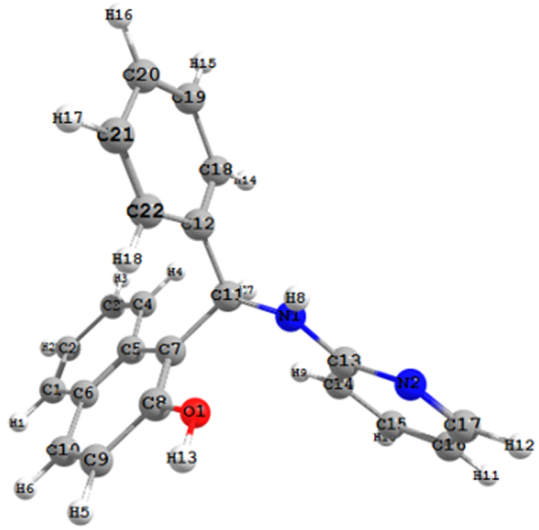

Fig. 1. The optimized structure of AMAN-1.

DNA structures and HSA to ensure an appropriate size for X-accessible space. The values of the centers of grid boxes are shown in Table 1. Other miscellaneous parameters were assigned to the default values given by the Autodock program. Finally, we obtained the dominating configuration of the AMAN-1 derivative with six DNA structures and HSA having minimum binding free energy (ΔG).

2.9. DNA binding experiments

2.9.1. UV–visible absorption spectral measurements

Absorbance spectra were recorded in the range (200–400 nm) with a spectrophotometer (Analytikjena specord 210) using a 1.0 cm quartz cell. Absorption titration experiments were carried out by keeping the concentration of AMAN-1 constant (3×10^{-5} M) while varying the DNA concentration from 0 to 3.69×10^{-5} M at room temperature.

2.9.2. Viscosity measurements

Viscosity measurements were made using a viscometer (SCHOT AVS 450) maintained at 25 °C in a constant temperature bath. The DNA concentration was fixed at 5×10^{-5} M and flow time was measured with a digital stopwatch; the mean values of three measurements were used to evaluate the viscosity (η) of the samples. The values for relative specific viscosity $(\eta/\eta_0)^{1/3}$, where η_0 and η are the specific viscosity contributions of DNA in the absence (η_0) and in the presence of the AMAN-1 (η), were plotted against 1/R (R = [AMAN-1]/[DNA] = 0.0–1.2).

3. Results and discussion

3.1. Characterization of molybdenum Schiff base complex immobilized on Fe_3O_4 nanoparticles

The most possible way for immobilization of molybdenum complex on the surface of chloro-modified magnetic nanoparticles are investigated. The hybrid materials obtained by mentioned method were characterized by Fourier transform infrared spectroscopy (FT-IR), X-ray diffraction (XRD), electron microscopy techniques (FESEM with EDS), vibrating sample magnetometer (VSM) and inductively coupled plasma (ICP).

The FT-IR spectra of Fe_3O_4 nanoparticles, Fe_3O_4@SiO_2, Fe_3O_4@SiO_2@MoSB and Mo Schiff base are shown in Fig. 2. The observation of broad bonds at around 470–740 cm^{-1} indicates the presence of Fe-O bond in Fe_3O_4 nanoparticles. The comparison of FT-IR spectra in Fig. 2, indicates the differences between uncoated and coated magnetic

Table 1
Five DNA sequences and HSA used for molecular docking.[a]

ID	PDB ID	Sequences	Unit Cell constants	Centers of grid boxes
1	1BNA	$D(CGCGAATTCGCG)_2$	a = 24.87 Å, b = 40.39 Å, c = 66.20 Å α = 90°, β = 90°, γ = 90°	14.719, 20.979, 8.824
2	1D32	D(CGCG)2	a = 16.88 Å, b = 26.88 Å, c = 82.60 Å α = 90°, β = 90°, γ = 90°	26.699, 13.011, 10.343
3	1DNE	$D(CGCGATATCGCG)_2$	a = 25.48 Å, b = 41.26 Å, c = 66.88 Å α = 90°, β = 90°, γ = 90°	15.259, 21.297, 75.998
4	1K2J	D(CGTACG)2	No data	0.218, 1.887, 7.463
5	1ZNA	D(CGCG)2	a = 31.27 Å, b = 64.67 Å, c = 19.50 Åα = 90°, β = 90°, γ = 90°	18.079, −8.217, 8.853
6	1AO6	HSA	a = 59.68 Å, b = 96.98 Å, c = 59.72 Åα = 91.07°, β = 103.50°, γ = 75.08°	29.535, 31.826, 23.5

[a] These data were extracted from Protein Data Bank (http://www.rcsb.org/pdb/home/home.do).

nanoparticles with silica. The bands appearing at 1064 cm^{-1} should be attributed to the stretching vibrations of the Si-O groups on the silica-coated nanoparticle. The weak bands at around 2915–2930 cm^{-1}, which are not present in IR spectrum of Fe_3O_4@SiO_2, assign to the stretching mode of the CH_2 groups of chlorosilane coupling agent. Also, the peak appeared at 1630 cm^{-1} in the IR spectrum of Mo Schiff base complex are related to C=N bond and confirm the synthesis of desired complex. In IR spectrum of final product, Fe_3O_4@SiO_2@MoSB, the vibration band at 1630 cm^{-1} is the typical IR absorbance for imine band [16].

The purity and crystalline structure of Fe_3O_4 nanoparticles and Fe_3O_4@SiO_2@MoSB were determined by powder X-ray diffraction (Fig. 3). The XRD pattern of Fe_3O_4 show eight peaks at 2θ = 18.3, 30.5, 35.9, 43.3, 53, 57, 62 and 74.5°, corresponding to Miller index values {h k l} of (1 1 1), (2 2 0), (3 1 1), (4 0 0), (4 2 2), (5 1 1), (4 4 0) and (5 3 3). As shown in Fig. 3b, the characteristic peaks of raw nanoparticles did not change, revealing that the structure of Fe_3O_4 is well maintained, after being coated with Mo Schiff base complex. A broad peak at 2θ = 20–30° representing the amorphous silica was also found besides the characteristic peaks of the Fe_3O_4 nanoparticles, which also indicated that magnetic nanoparticles had been successfully encapsulated by silica-layered systems. The average crystal size of the final nanoparticles is calculated using the Scherrer equation for immobilized Schiff base complexes which is found to be approximately 18 nm [35].

The morphology of the synthesized Fe_3O_4@SiO_2@MoSB was studied by scanning electron microscopy technique. SEM images of the catalyst at two different magnifications with the scale bar of 500 nm (Fig. 4a) and 100 nm (Fig. 4b) were recorded. These images clearly show that nanoparticles have been formed and are well-defined spherical particles. The size of synthesized nanomaterials was in the range of 10–30 nm.

The elemental composition was determined using Energy-dispersive X-ray (EDX) analysis. Fig. 4c shows the EDX pattern of catalyst, indicating that it is composed of iron, carbon, silicon, nitrogen, oxygen and chlorine elements. In addition to the mentioned peaks, the characteristic peaks of molybdenum support the possible complexation of molybdenum with Schiff base moieties. This result confirms the successful immobilizing of the Schiff base sites on the surface of magnetic nanoparticles.

Magnetic properties of prepared materials have been investigated at room temperature by means of vibrating sample magnetometry (VSM). According to Fig. 5, it can be seen that all samples show excellent superparamagnetic properties, indicating the retaining of the nanostructural nature of Fe_3O_4 during immobilizing presses. The saturation magnetization values for Fe_3O_4 and Fe_3O_4@SiO_2@MoSB nanocomposites are 48 and 38 $emug^{-1}$, respectively. Compared with neat nanoparticles, a decrease of about 10 $emug^{-1}$ in saturation magnetization value was observed for supported nanoparticles which can be attributed to the coating of the magnetite particles with silica, organic groups and Schiff base complex. However, the catalyst could still be separated comfortably from the reaction mixture by using an external magnet.

Finally, the amount of Mo in the supported catalyst, determined by ICP, was about 0.29 mmol g^{-1}.

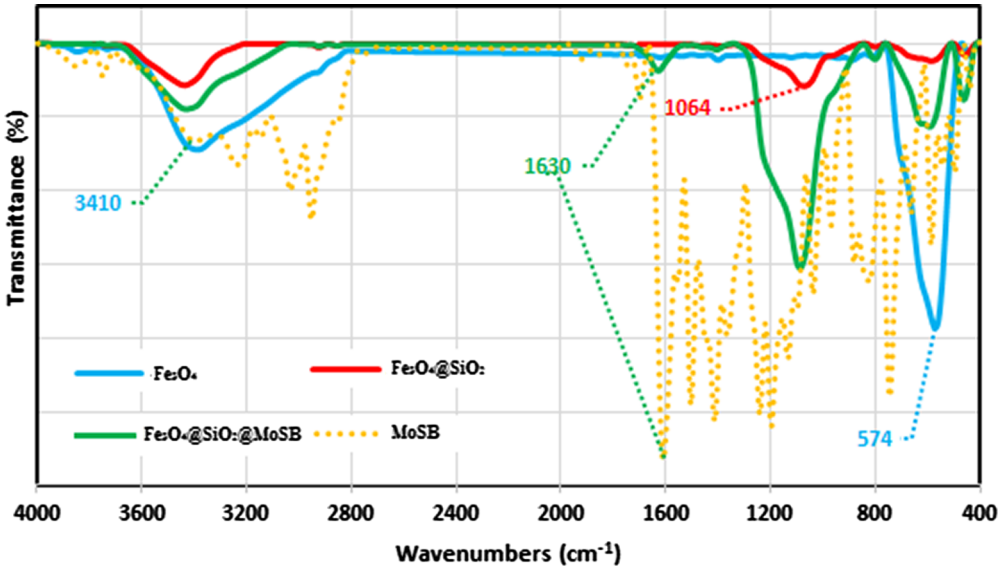

Fig. 2. FT-IR Spectra of Fe_3O_4 (blue), Fe_3O_4@SiO_2 (red), Fe_3O_4@SiO_2@MoSB (green) and Mo Schiff base (dashed line).

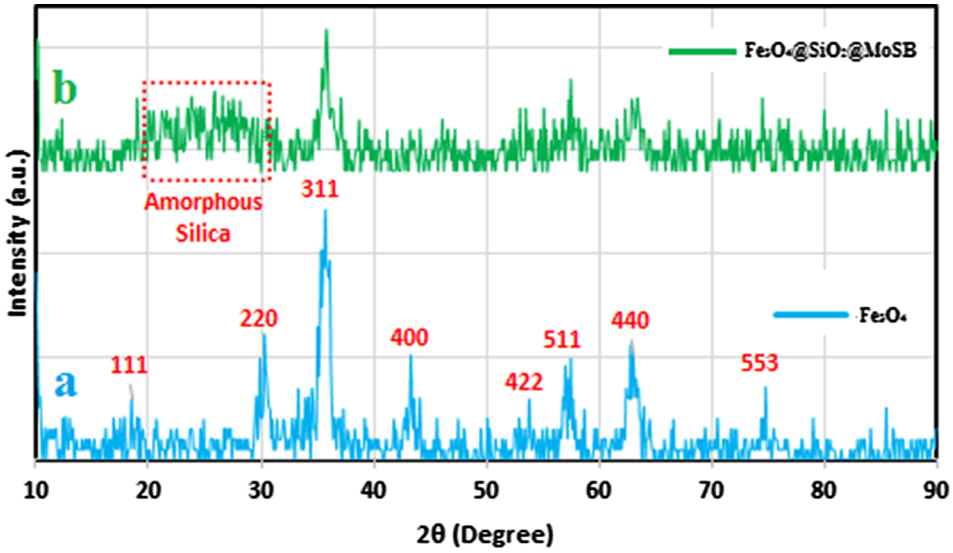

Fig. 3. Wide angle XRD patterns of the different samples. Different planes are indexed.

3.2. Application of molybdenum complex immobilized on Fe_3O_4 as a heterogeneous catalyst

The catalytic activity of the Mo complex immobilized on nanoparticles as a mild and efficient acid catalyst was applied in the one-pot three component condensation of aromatic aldehydes, 2-, 3- or 4-aminopyridine and β-naphthol for the synthesis of 1-(α-aminoalkyl)-2-naphthol derivatives under ultrasonic irradiation. At the first stage, to find out the optimum parameters including the quantity of catalyst, solvent and temperature, we studied the reaction of β-naphthol (1),

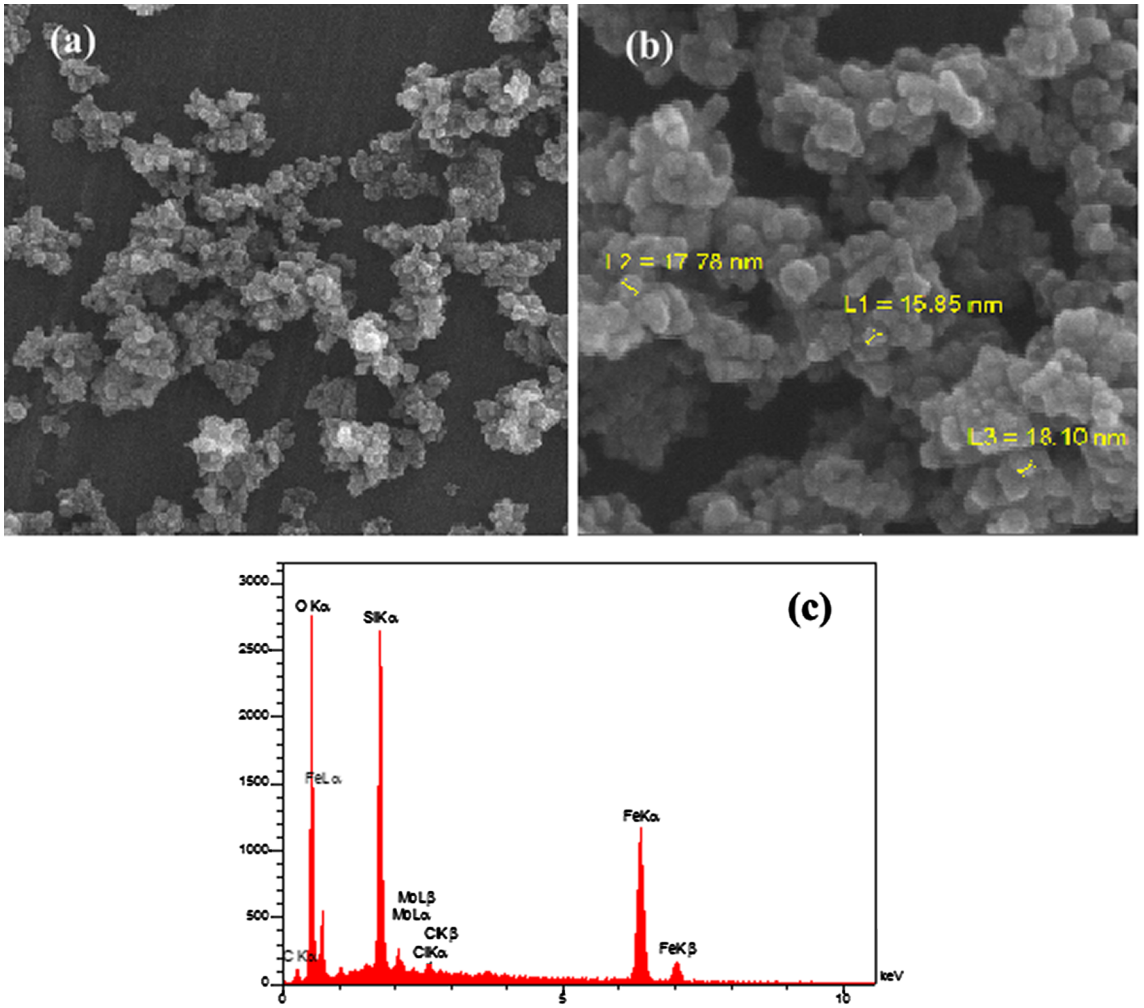

Fig. 4. FE-SEM micrograph with the scale bar of 500 nm (a), 100 nm (b) and EDX spectrum of Fe_3O_4@SiO_2@MoSB (c).

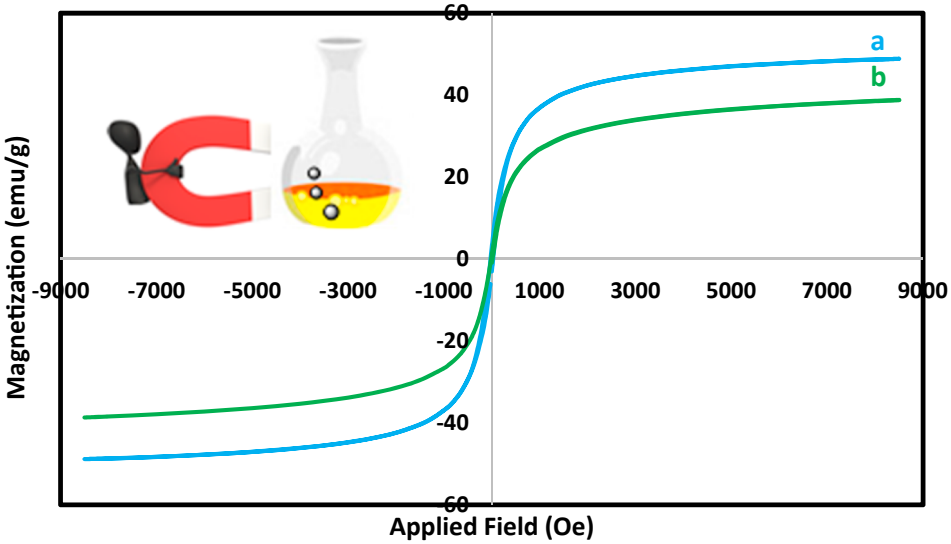

Fig. 5. Magnetic hysteresis curves measured at room temperature for Fe_3O_4 (a, blue) and Fe_3O_4@SiO_2@MoSB (b, green).

naphthalene-1-carbaldehyde (2) and 2-aminopyridine (3) as a model reaction in various conditions.

We try to screen the effect of catalyst amount on the reaction and yields. As shown in Table 2, the result shows that in the absence of catalyst a trace amount of product was observed over a period of 45 min and the best result was achieved when we carried out the model reaction in the presence of 6 mg of catalyst. In order to check the effect of temperature on the reaction, the range of 25–100 °C was screened. It was observed that in the presence of 6 mg of catalyst the yield of product has no change when we increase the reaction temperature up to 100 °C (Table 2, entries 7–10). To verify the effect of ultrasound irradiation on this procedure, the synthesis of 1-(α-aminoalkyl)-2-naphthols was done in the presence of varying amount of the nanocatalyst with and without ultrasound irradiation (Table 3). It is clear that, reactions under ultrasonic irradiation led to shorter reaction times and higher yields. It continued to optimize the model reaction by detecting the effect of various solvents as the medium by using nanocatalyst at room temperature. The represented data in Table 4, showed the reaction without any solvent was very successful with good high yields. Therefore, the best results from the model reaction were obtained in the presence of 6 mg of nanocatalyst at room temperature, solvent-free and ultrasonic irradiation conditions.

Having established the remarkable results, and in order to show the generality of these conditions to other substrates, a variety of 1-(α-aminoalkyl)-2-naphthol derivatives were synthesized from the three component reaction of different kinds of aromatic aldehydes containing electron-donating or electron-withdrawing functionalities (1 mmol), 2-, 3- or 4-aminopyridine (1 mmol) and β-naphthol (1 mmol) employing combined ultrasonic/Mo Schiff base complex immobilized on Fe_3O_4 nanoparticles (6 mg) as the heterogeneous acid catalyst under solvent-free reaction condition. The results have been summarized in Table 5. According to the results, all the reactions proceeded equally smooth and afforded the desired products in excellent yields and short reaction time irrespective of the nature of the substituents. It should be noted that, aldehydes with electron-withdrawing group and cinnamaldehyde were rather faster than electron donating groups and worked well under these conditions. According to the ICP results for metal content, (6 mg of catalyst is equivalent to 0.17 mol% of catalyst), turn over number (TON) and turn over frequency (TOF) of the catalyst were calculated. The amount of metals loaded on magnetic support determined by

Table 2
Effects of catalyst concentration and temperature on the synthesis of 1-(α-aminoalkyl)-2-naphthols derivatives under solvent-free conditions.[a]

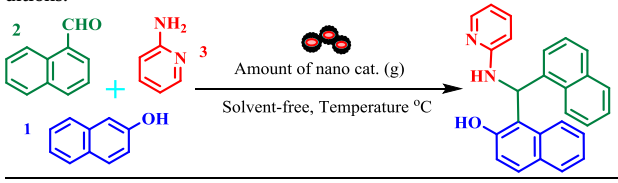

Entry	Amount of catalyst (mg)	Reaction temperature (°C)[b]	Reaction time (min)	Yield[c] (%)
1	–	r.t.	45	30
2	–	100	45	30
3	2	r.t.	45	45
4	2	100	45	50
5	4	r.t.	45	75
6	4	100	45	77
7	6	r.t.	20	94
8	6	50	20	94
9	6	75	20	94
10	6	100	20	94
11	8	r.t.	20	94
12	8	50	20	94
13	8	75	20	94
14	8	100	20	94
15	10	r.t.	20	95
16	10	100	20	95

[a] Reaction conditions: naphthalene-1-carbaldehyde (1 mmol), β-naphthol (1 mmol) and 2-aminopyridine (1 mmol) under ultrasonic irradiation.
[b] This is the temperature of oil bath and not inside the reaction medium.
[c] Isolated yield.

Table 3
Effect of amounts of catalyst with or without sonication for synthesis of 1-(α-aminoalkyl)-2-naphthol derivatives under solvent-free conditions.[a]

Entry	Amount of catalyst (mg)	With sonication		Without sonication	
		Yield (%)	Time (min)	Yield (%)	Time (min)
1	2	30	45	16	70
2	4	75	45	50	55
3	6	94	20	65	40
4	8	94	20	65	40
5	10	94	20	65	40

[a] Reaction conditions: naphthalene-1-carbaldehyde (1 mmol), β-naphthol (1 mmol) and 2-aminopyridine (1 mmol).

Table 4
Effects of solvent on the synthesis of 1-(α-aminoalkyl)-2-naphthol derivatives using 6 mg catalyst at room temperature.

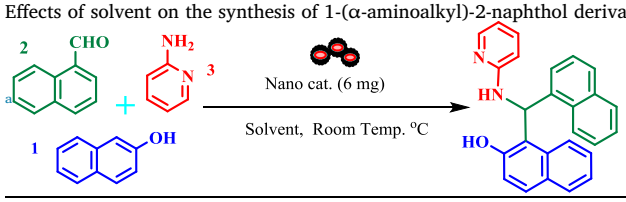

	Solvent-free	H_2O	C_2H_5OH	CH_3CN	CH_2Cl_2	Toluene	*n*-Hexane
Yield (%)[b]	94	35	70	60	50	30	35
Reaction time (min)	20	40	45	40	35	50	60

[a] Naphthalene-1-carbaldehyde (1 mmol), β-naphthol (1 mmol) and 2-aminopyridine (1 mmol) by under ultrasonic irradiation under room temperature.
[b] Isolated yield.

atomic absorption spectrophotometer.

To explore the scope and generality of this combined catalytic system, different kinds of aldehydes (1) reacted with TMSCN (2) and aniline (3) to produce a library of α-aminonitrile derivatives (4) under the same conditions. As can be seen from Table 6, the progress of this reaction was checked by TLC and the corresponding compounds were obtained in excellent yields. Therefore, the important role of the catalyst and ultrasonic irradiation in the reaction was verified.

Due to the lack of research articles on the synthesis of 1-(α-aminoalkyl)-2-naphthol derivatives with aforementioned substrates, a limited comparison between the efficiency of our method and other reported procedures in the synthesis of the same titled products was possible. The results for the preparation of 1-(p-Chlorophenyl(2-pyridinylamino)methyl)naphthalene-2-ol were represented in Table 7. We can conclude that our procedure is in the first rank among all methods in terms of the reaction time and yield and also this fact that it avoids the use of volatile organic solvents in the reaction. So it shows that use of the ultrasound irradiation improves the rate of reaction and also yields of products formed.

In addition, the reusability of our catalyst was investigated for the condensation of β-naphthol and naphthalene-1-carbaldehyde with 2-aminopyridine. After completion of the reaction, the catalyst was separated with magnet in hot condition, after washing with ethanol, dried at 60 °C and reused for a similar reaction. The recovered catalyst could be reused at least eight times without significant loss of activity (Fig. 6). Furthermore, the FT-IR spectrum and XRD pattern of the reused catalyst after eight cycles revealed that the structure of the catalyst maintains during the reactions.

A proposed mechanism for synthesis of 1-aminoalkyl-2-naphthol derivatives in the presence of the Mo Schiff base complex immobilized on Fe_3O_4 nanoparticles has been presented in Scheme 3. In this mechanism, at first, the nanocatalyst activates the carbonyl group of the

Table 5
The three-component synthesis of 1-(α-aminoalkyl)-2-naphthol derivatives using 6 mg of nanocatalyst.

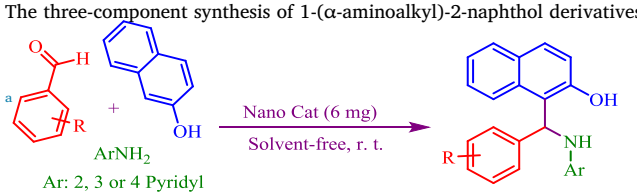

Name	R	Ar	Time (min)	Yield[b] (%)	TON[c]	TOF (min^{-1})[d]	M.p (°C) [Ref.]
AMAN-1	H	2-Pyridyl	12	96	564.70	47.05	170–172 [29]
AMAN-2	4-NO_2	2-Pyridyl	10	97	570.58	57.05	192–194 [30]
AMAN-3	4-Cl	2-Pyridyl	10	96	564.70	56.47	188–190 [27]
AMAN-4	4-Br	2-Pyridyl	15	90	529.41	35.29	210–212 [27]
AMAN-5	2,4-Cl	2-Pyridyl	10	95	558.82	55.88	177–179[e]
AMAN-6	4-CH_3	2-Pyridyl	20	88	517.64	25.88	172–174 [27]
AMAN-7	4-OCH_3	2-Pyridyl	20	85	500.00	25.00	168–170 [30]
AMAN-8	1-Naphtyl	2-Pyridyl	20	94	552.94	27.64	220–222 [30]
AMAN-9	H	3-Pyridyl	20	87	511.76	25.58	166–168 [31]
AMAN-10	4-NO_2	3-Pyridyl	10	92	541.17	54.11	200–202 [31]
AMAN-11	4-Cl	3-Pyridyl	15	88	517.64	34.50	182–184 [31]
AMAN-12	4-Br	3-Pyridyl	25	90	529.41	21.17	211–213 [31]
AMAN-13	4-NO_2	4-Pyridyl	15	96	564.70	37.64	285–287 [30]
AMAN-14	4-Cl	4-Pyridyl	10	96	564.70	56.47	223–225 [30]
AMAN-15	4-CH_3	4-Pyridyl	15	90	529.41	35.29	218–220 [30]
AMAN-16	4-OCH_3	4-Pyridyl	15	89	523.52	34.90	257–259 [30]
AMAN-17	1-Naphtyl	4-Pyridyl	12	90	529.41	44.11	260–262 [30]
AMAN-18	H	Ph	25	88	517.64	20.70	200–202 [29]
AMAN-19	3-NO_2	Ph	30	91	535.29	17.74	232–234 [29]
AMAN-20	4-Cl	Ph	30	87	511.76	17.05	183–185 [29]
AMAN-21	4-Br	Ph	40	86	505.88	12.64	190–192 [29]

[a] Reaction conditions: Aldehyde (1 mmol), *β*-naphthol (1 mmol), 2, 3 or 4 aminopyridine (1 mmol), room temperature, solvent-free; ultrasonic irradiation.
[b] Isolated yield.
[c] Turnover numbers (TONs).
[d] Turnover frequencies (TOFs).
[e] New derivative.

Table 6
The three-component synthesis of α-aminonitrile derivatives using 6 mg of nano catalyst.[a]

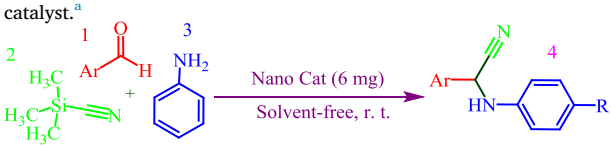

Entry	Ar	Time (min)	Yield[b] (%)	TON[c]	TOF (min^{-1})[d]	M.p (°C) [Ref.]
1	C_6H_5	25	85	500.00	20.00	80–83 [40]
2	4-ClC_6H_5	20	89	523.52	26.17	117–119 [40]
3	4-$NO_2C_6H_5$	20	90	529.41	26.47	Oil [40]
4	4-$CH_3C_6H_5$	30	85	500.00	16.66	78–80 [40]
5	4-$CH_3OC_6H_5$	30	88	517.64	17.25	93–95 [40]
6	4-CNC_6H_5	25	90	529.41	21.17	105–107 [40]

[a] Reaction conditions: Aldehyde derivatives (1 mmol), aniline (1 mmol), TMSCN (1 mmol), room temperature, solvent-free, ultrasonic irradiation.
[b] Isolated yield.
[c] Turnover number (TON).
[d] Turnover frequency (TOF).

Table 7
Comparison of the Fe_3O_4@SiO_2@MoSB catalytic activity with those of reported procedures.[a]

Catalyst	Solv.	Temp (°C)	Time (min)	Yield[b] (%)	[Ref.]
MNP-$PhSO_3H$	–	120	15	85	[29]
{[1,4-DHPyrazine][$C(NO_2)_3$]$_2$}	–	r.t.	15	96	[30]
Absence of catalyst	–	125	5	90	[31]
Absence of catalyst	H_2O	r.t.	40	98	[27]
Fe_3O_4@SiO_2@MoSB	–	r.t.	8	96	This work

[a] Model reaction:4-chlorobenzaldehyde, β-naphthol and 2-aminopyridine.
[b] Isolated yield.

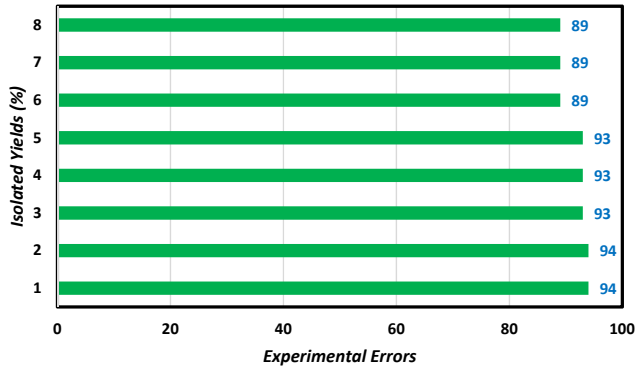

Fig. 6. Reusability of Fe_3O_4@SiO_2@MoSB as a heterogeneous catalyst in model reaction.

aromatic aldehyde to give intermediate (I). In the second step, β-naphthol attacks the intermediate (I) by the nucleophilic addition affording the corresponding intermediate II as an ortho-quinone methide (o-QM). The mechanism ends with the reaction of o-quinone methide with amines to form the aminoalkyl naphthol derivatives [29,41].

3.3. In vitro mechanism action study of one type of derivatives with DNA

Generally, drug molecules can bind with DNA by means of either covalent or non-covalent interactions. For these interactions, there are different binding sites in the DNA molecule: (i) between any two nitrogen base pairs (intercalation binding), (ii) in the major or minor groove (groove binding), (iii) on the exterior side of the helix (electrostatic binding) [42]. In the present study, to attain a better understanding of mechanism action of 1-(phenyl(pyridin-2-ylamino)methyl) naphthalen-2-ol (AMAN-1) with ct-DNA, UV–visible absorption spectroscopy and viscosity measurement was investigated.

3.3.1. UV–vis absorption studies

In UV–Vis absorption spectroscopy technique, hyperchromism and hypochromism are the generally meaningful spectral properties, which are used to discriminate against the variations in the structure of DNA double-helix. Hypochromism is observed when there is a close proximity interaction between the electronic levels of the interacting chromophore and those of the nitrogen atoms of DNA base pairs [43]. Fig. 7 shows the UV–Vis absorption spectra of AMAN-1 (5×10^{-5} M) in the absence and presence of different concentrations of ct-DNA (0 to 3.69×10^{-5} M). The absorption peak of AMAN-1 showed a gradual decrease with the increasing of different concentrations of ct-DNA. Furthermore, in order to obtain a more quantitative determination of the interaction strength between AMAN-1 and ct-DNA, intrinsic binding constant, K_b, was determined using spectroscopic titration data at 260 nm. Then the data were fitted to Eq. (1) to obtain the binding constant [44]:

$$\frac{\varepsilon_a - \varepsilon_f}{\varepsilon_b - \varepsilon_f} = \frac{b - (b^2 - \frac{2k_b^2 C_t [DNA]}{s})^{\frac{1}{2}}}{2k_b C_t}$$
$$b = 1 + k_b C_t + \frac{k_b [DNA]}{2s} \quad (1)$$

where ε_a is the extinction coefficient observed for AMAN-1 absorption band at a given DNA concentration, ε_f is the extinction coefficient of the free derivative in solution, ε_b is the extinction coefficient of the derivative when fully bound to DNA (it is assumed when further addition of DNA does not change the absorbance, all the AMAN-1 molecule is bound and ε_b can be calculated from Beer's Law), K_b is the equilibrium binding constant, C_t is the total AMAN-1 concentration in nucleotide, and s is the binding site size. The plots of $(\varepsilon_a - \varepsilon_f)/(\varepsilon_b - \varepsilon_f)$ versus [DNA] is shown in Fig. 8. The calculated K_b value was 2.9×10^5 M^{-1}.

3.3.2. Viscosity measurements

To further verify the interaction binding mode between the AMAN-1 and ct-DNA, viscosity measurements were carried out. Generally, the classical intercalator compounds cause an increase in the DNA viscosity (separates base pairs of DNA in order to accommodate the binding ligand). Non-classical compounds (such as groove binding and electrostatic) cause the reduction or no change in the DNA viscosity [45]. The effect of the AMAN-1 on the viscosity of DNA is illustrated in Fig. 9. As can be seen, the viscosity of DNA increased slightly or remained constant with increasing different amounts of AMAN-1. This behavior may reveal the existence of groove binding mode between DNA and the AMAN-1. This result is consistent with molecular docking results (Sections 3–4).

3.4. Molecular docking study of one type of derivatives with different type of DNAs

3.4.1. Molecular docking study with DNA

Molecular docking is a well-established computational method to identify the drug–macromolecule (such as DNA and HSA) interactions for designing the modern drugs and to predict the specific binding site available at the molecular target [46–50]. In the present study, molecular docking studies of AMAN-1 with different types of DNA were performed in an attempt to ascertain the preferred orientation of this derivative inside the DNA sequence (Fig. 10). The AMAN-1 molecule was docked into various types of rigid DNA and the results were listed in Table 8. The values of electrostatic forces between the drug candidate and DNAs is much lower than the sum of the hydrogen bonding

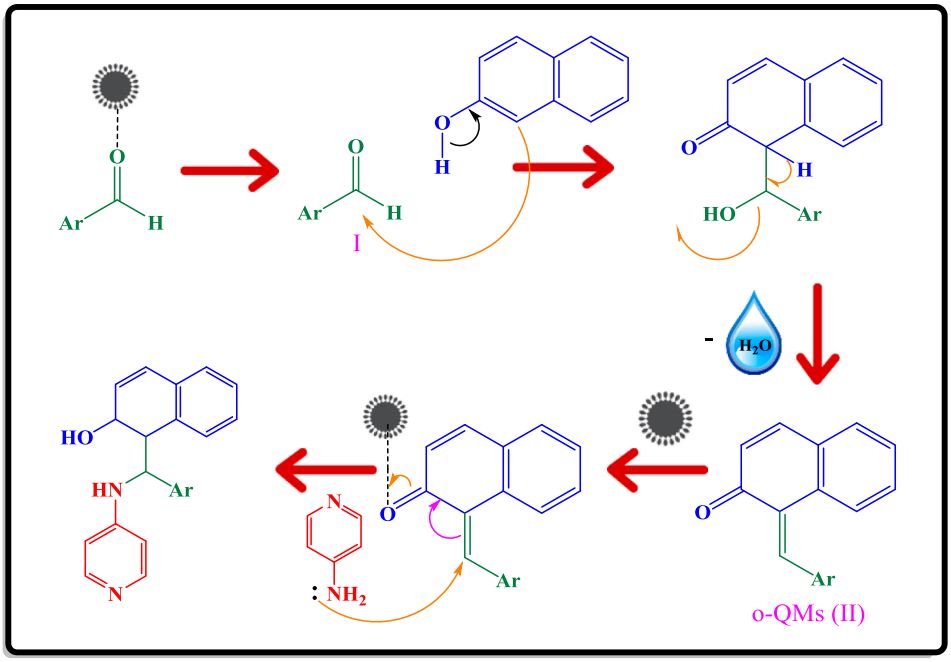

Scheme 3. Proposed mechanism for the synthesis of 1-(α-aminoalkyl)-2-naphthol derivatives using molybdenum complex supported on functionalized Fe_3O_4 magnetite nanoparticles.

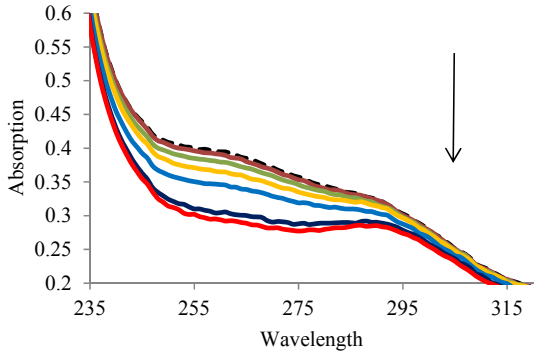

Fig. 7. Absorption spectra of AMAN-1 in the presence of ct-DNA at different concentrations. Conditions: c(AMAN-1) = 5.0×10^{-5} mol L^{-1}. c(DNA) ($\times 10^{-5}$ mol L^{-1}): 0.53, 1.06, 1.60, 2.12, 2.64 and 3.69 pH = 7.4.

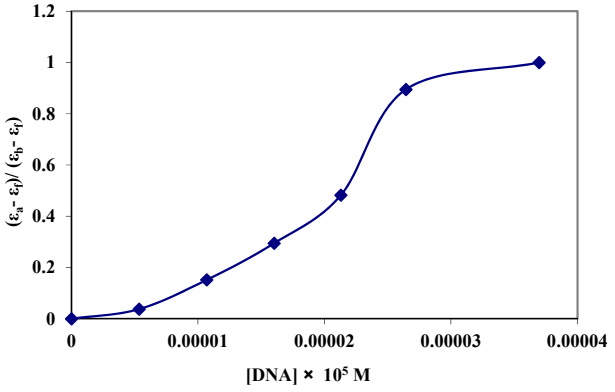

Fig. 8. Plots of $(\varepsilon_a - \varepsilon_f)/(\varepsilon_b - \varepsilon_f)$ versus [DNA] for the titration of AMAN-1 with ct-DNA.

energy, van der Waals energy and desolvation free energy in the binding process of DNA sequence and AMAN-1, and from this result, it can be concluded that the main binding mode between the desired

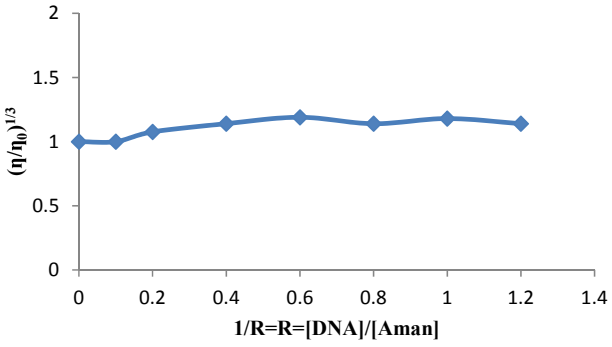

Fig. 9. Effect of increasing the concentration of AMAN-1 on the relative viscosity of ct-DNA at 25 °C.

derivative and DNAs is not electrostatic.

3.4.2. Molecular docking study with HSA

To determine the binding ability of the AMAN-1 with the HSA (PDB ID: 1AO6), molecular docking studies were performed. Generally, crystal structure descriptions of the 3D structure of HSA showed that a single polypeptide chain of 585 amino acid residues contains three structurally homologous domains (I–III): I (residues 1–195) II (196–383) and III (384–585); each domain has two subdomains (A and B) [51]. In addition, the drug binding sites of HSA are located in tryptophan residue (Trp-214) of HSA in subdomain IIA and hydrophobic cavities in subdomain IA and IIA respectively. The molecular docking pattern of AMAN-1 and HSA indicated that HSA/AMAN-1 complex was located in the subdomains IIA of HSA and also hydrogen binding and hydrophobic interactions play an important role in the stability of this complex (Fig. 11).

4. Conclusions

In conclusion, we have synthesized and characterized a heterogeneous catalyst by immobilizing a Mo Schiff base complex onto silica-coated magnetic Fe_3O_4 nanoparticles to overcome the leaching of the

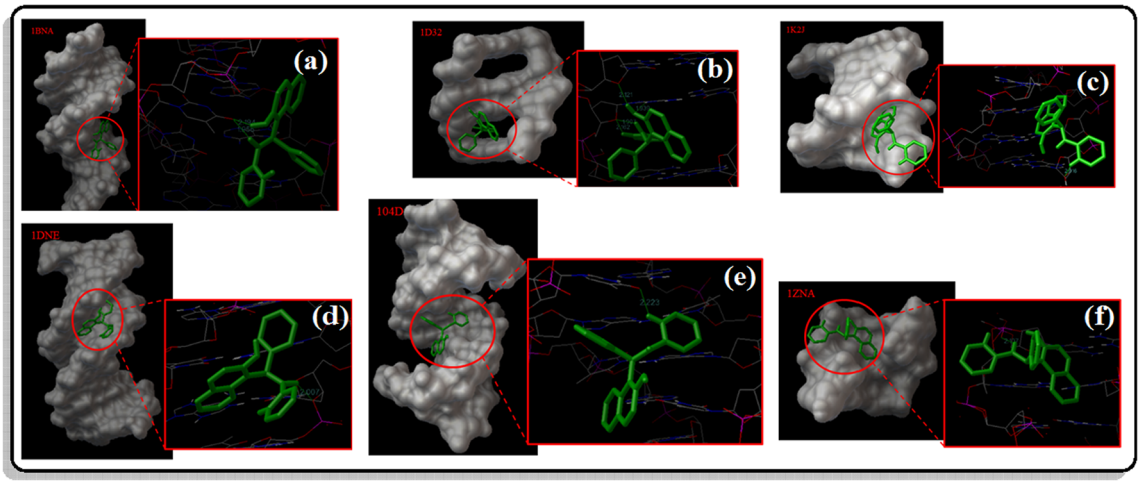

Fig 10. Molecular docking of the interactions of 1BNA (a), 1D32 (b), 1K2J (c), 1DNE (d), 104D (e) and 1ZNA (f) as a type of DNA with AMAN-1.

complex in reaction medium. A new synthetic method for the synthesis of 1-aminoalkyl-2-naphthol derivatives using the aforesaid catalyst in room temperature and solvent-free condition have been developed. Then, to establish the generality of this procedure, we have also extended this protocol for the synthesis of α-aminonitriles. The nanocatalyst synthesized here is stable to the reaction conditions and can be recycled without significant loss of activity. Comparison of the procedure efficiency of our combined method with other catalysts and reaction conditions used in previous works indicates that our reaction condition have merits over other reactions in several aspects. Finally, we tried to have a new viewpoint of the mechanism of interaction between one type of aminoalky naphthol derivatives with DNA, that helps us to design new molecular models of both novel and more efficient drug molecules which treat DNA. The results of UV–vis absorption spectroscopy and viscosity measurements indicated that the selected

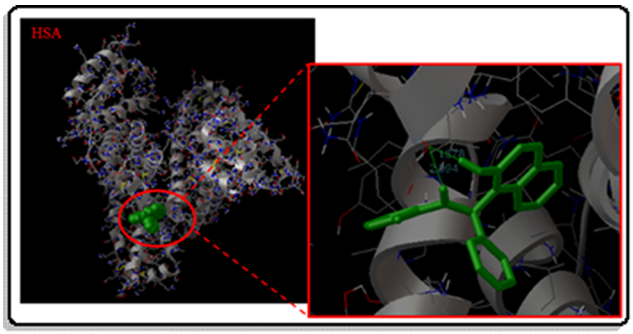

Fig 11. Molecular docking of the interaction of HSA with AMAN-1.

Table 8
The various energies and the hydrogen bonding interactions in the formation process of DNAs/AMAN-1 and HAS/AMAN-1 complexes.

PDB ID	$\Delta G^0_{(a)}$ kcal mol^{-1}	$\Delta E_{1(b)}$ kcal mol^{-1}	$\Delta E_{2(c)}$ kcal mol^{-1}	Hydrogen bonding			Binding site
				DNA	AMAN	Bond length(Å)	
1BNA	−7.17	−8.66	−0.10	DT7:O4 (Chain A)	O1:H13	2.194	Major groove
				DT7:O4 (Chain A)	N1:H8	1.196	
1D32	−7.72	−9.21	−0.09	C7:O4* (Chain B)	O1:H13	2.121	Intercalation
				G6:H3 (Chain B)	O1	1.939	
				G6:O4* (Chain B)	N1:H8	1.907	
				G6:O4* (Chain B)	N2	2.162	
1DNE	−8.84	−10.33	−0.19	T18:O3* (Chain B)	N1:H8	2.00	Minor groove
1K2J	−6.47	−7.96	−0.05	G12:O3* (Chain B)	N2	2.01	Major groove
1ZNA	−7.45	−8.94	−0.09	G6:O1P (Chain B)	N1:H8	2.10	Major groove
104D	−6.57	−8.06	−0.10	DT17:O4 (Chain B)	N1:H8	2.22	Major groove
1AO6	−7.82	−9.31	−0.02	SER480(OG) (Chain A)	O1:H13	1.878	IIA
				SER480(OG) (Chain A)	N1:H8	2.094	IIA

(a) ΔG^0 is the binding free energy change in the binding process. (b) ΔE_1 denotes intermolecular interaction energy, which is a sum of van der Waals energy, hydrogen bonding energy, desolvation free energy and electrostatic energy. (c) ΔE_2 is the electrostatic energy.

aminoalkynaphthol derivative interacts with ct-DNA in an intercalative binding mode, and the binding constant is 2.9×10^5 M^{-1}. Also, the result of molecular modeling was in approximate correlation with our experimental results.

Acknowledgements

We would like to thank University of Tabriz and Iran National Science Foundation (INSF) (Grant Number: 95014554) for financial support to our research group.

References

[1] S. Shylesh, V. Schunemann, W.R. Thiel, Angew. Chem. Int. Ed. 49 (2010) 3428–3459.
[2] Q. Du, W. Zhang, H. Ma, J. Zheng, B. Zhou, Y. Li, Tetrahedron 68 (2012) 3577–3584.
[3] R.B.N. Baig, R.S. Varma, Chem. Commun. 48 (2012) 2582–2584.
[4] H. Hamadi, M. Kooti, M. Afshari, Z. Ghiasifar, N. Adibpour, J. Mol. Catal. A. Chem. 373 (2013) 25–29.
[5] N.E. Leadbeater, M. Marco, Chem. Rev. 102 (2002) 3217–3274.
[6] S. Minakata, M. Komatsu, Chem. Rev. 109 (2009) 711–724.
[7] N. Koukabi, E. Kolvari, A. Khazaei, M.A. Zolfigol, B. Shirmardi-Shaghasemic, H.R. Khavasi, Chem. Commun. 47 (2011) 9230–9232.
[8] K. Turcheniuk, A.V. Tarasevych, V.P. Kukhar, R. Boukherroub, S. Szunerits, Nanoscale 5 (2013) 10729–10752.
[9] T. Katsuki, Coord. Chem. Rev. 140 (1995) 189–214.
[10] M. Esmaeilpour, A.R. Sardarian, J. Javidi, App. Catal. A: Gen. 445 (2012) 359–367.
[11] P.G. Cozzi, Chem. Soc. Rev. 33 (2004) 410–421.
[12] K.C. Gupta, A.K. Sutar, Coord. Chem. Rev. 252 (2008) 1420–1450.
[13] V. Mirkhani, S. Tangestaninejad, M. Moghadam, M. Moghbel, Bioorg. Med. Chem. 12 (2004) 903–906.
[14] W. Zhang, J.L. Loebach, S.R. Wilson, E.N. Jacobsen, J. Am. Chem. Soc. 112 (1990) 2801–2803.
[15] S.B. Routier, J.L. Bernier, M.P. Catteau, C. Bailly, Bioorg. Med. Chem. Lett. 7 (1997) 63–66.
[16] J. Rakhtshah, S. Salehzadeh, E. Gowdini, F. Maleki, S. Baghery, M.A. Zolfigol, RSC Adv. 6 (2016) 104875–104885.
[17] K.C. Gupta, A.K. Sutara, C.C. Lin, Coord. Chem. Rev. 253 (2009) 1926–1946.
[18] S. Das, S. Bhunia, T. Maity, S. Koner, J. Mol. Catal. A. Chem. 394 (2014) 188–197.
[19] N. Anand, K.H.P. Reddy, V. Swapna, K.S.R. Rao, D.R. Burri, Micropor. Mesopor. Mater. 143 (2011) 132–140.
[20] M. Bagherzadeh, M. Zare, M. Amini, T. Salemnousha, S. Akbayrak, S. Ozkar, J. Mol. Catal. A. Chem. 395 (2014) 470–480.
[21] M.B. Gawande, Y. Monga, R. Zborila, R.K. Sharma, Coord. Chem. Rev. 288 (2015) 118–143.
[22] C. Cardellicchio, M.A.M. Capozzi, F. Naso, Tetrahedron Asymmetry 21 (2010) 507–517.
[23] J. Lu, X. Xu, C. Wang, J. He, Y. Hu, H. Hu, Tetrahedron Lett. 43 (2002) 8367–8369.
[24] S. Knapp, Chem. Rev. 95 (1995) 1859–1876.
[25] Y.F. Wang, T. Izawa, S. Kobayashi, M. Ohno, J. Am. Chem. Soc. 104 (1982) 6465–6466.
[26] F. Ma, L. Shen, X. Ai, C. Zhang, Org. Lett. 9 (2007) 125–127.
[27] M. Ghandi, A. Olyaei, S. Raoufmoghaddam, Synth. Commun. 38 (2008) 4125–4138.
[28] I. Szatmari, F. Fulop, F. Synthesis 5 (2009) 775–778.
[29] H. Moghanian, A. Mobinikhaledi, A.G. Blackman, E. Sarough-Farahani, RSC Adv. 4 (2014) 28176–28185.
[30] M.A. Zolfigol, S. Baghery, A.R. Moosavi-Zare, S.M. Vahdat, J. Mol. Catal. A. Chem. 409 (2015) 216–226.
[31] A. Olyaei, S. Raoufmoghaddam, M. Sadeghpour, B. Ebadzadeh, Chin. J. Chem. 28 (2010) 825–832.
[32] A. Kumar, M.K. Gupta, M. Kumar, Tetrahedron Lett. 51 (2010) 1582–1584.
[33] J. Rakhtshah, S. Salehzadeh, Appl. Organometal. Chem. 31 (e3560) (2017) 1–9.
[34] J. Rakhtshah, S. Salehzadeh, S. Baghery, M.A. Zolfigol, J. Coord. Chem. 70 (2017) 340–360.
[35] J. Rakhtshah, S. Salehzadeh, Res. Chem. Intermed. 43 (2017) 6973–6991.
[36] M. Ma, Y. Zhang, W. Yu, H.Y. Shen, H.Q. Zhang, N. Gu, Colloids Surf., A 212 (2003) 219–226.
[37] W. Stober, A. Fink, E.J. Bohn, J. Colloid Interface Sci. 26 (1968) 62–69.
[38] http://www.hyper.com.
[39] G.M. Morris, D.S. Goodsell, R.S. Halliday, R. Huey, W.E. Hart, R.K. Belew, A.J. Olson, Autodock, version 4.0.1, The Scripps Research Institute, LaJolla, CA, USA, 2007.
[40] M.G. Dekamin, Z. Mokhtari, Z. Karimi, Sci. Iran. 18 (2011) 1356–1364.
[41] A. Chinnappan, A.H. Jadhav, W.J. Chung, H. Kim, J. Mol. Liq. 212 (2015) 413–417.
[42] Y. Ni, D. Lin, S. Kokat, Anal. Biochem. 352 (2006) 231–242.
[43] (a) G.W. Zhang, P. Fu, L. Wang, M.M. Hu, J. Agric, Food Chem. 59 (2011) 8944–8952;
(b) X.L. Li, Y.J. Hu, Biomacromol 13 (2012) 873–880.
[44] N. Shahabadi, Z. Mirzaei kalar, N. Hosseinpour Moghadam, Spectrochim. Acta A. Mol. Biomol. Spectrosc. 96 (2012) 723–728.
[45] Z. Kazemi, H. Amiri Rudbari, M. Sahihi, V. Mirkhani, M. Moghadam, S. Tangestaninejad, I. Mohammadpoor-Baltork, G. Azimi, S. Gharaghani, A. Abbasi Kajani, J. Photochem. Photobiol. B. 163 (2016) 246–260.
[46] M. Taha, M. Arbin, N. Ahmat, S. Imran, F. Rahim, Bioorg. Chem. 77 (2018) 47–55.
[47] M. Taha, S.A. Ali Shah, M. Afifi, S. Imran, S. Sultan, F. Rahim, K.M. Khan, Bioorg. Chem. 77 (2018) 586–592.
[48] U. Salar, K.M. Khan, S. Chigurupati, M. Taha, A. Wadood, S. Vijayabalan, M. Ghufran, S. Perveen, Sci. Rep. 7 (2017) 16980.
[49] W. Jamil, D. Kumari, M. Taha, M.N. Khan, M.S. Baharudin, M. Ali, M. Kanwal, M.S. Lashari, K.M. Khan, J. Iran. Chem. Soc. 15 (2018) 2441–2454.
[50] M. Yara, M. Bajdab, S. Shahzad, N. Ullah, M.A. Gilani, M. Ashra, A. Rauf, A. Shaukat, Bioorg. Chem. 58 (2015) 65–71.
[51] (a) X.M. He, D.C. Carter, Nature 358 (1992) 209–215;
(b) K. Yamasaki, V.T.G. Chuang, T. Maruyam, M. Otagiri, Biochim. Biophys. Acta 1830 (2013) 5435–5443.